Journal of The Electrochemical Society, **159** (9) F554-F559 (2012)
0013-4651/2012/159(9)/F554/6/$28.00 © The Electrochemical Society

Atomic-Scale Compositional Mapping and 3-Dimensional Electron Microscopy of Dealloyed $PtCo_3$ Catalyst Nanoparticles with Spongy Multi-Core/Shell Structures

Zhongyi Liu,[a,z] Huolin Xin,[b] Zhiqiang Yu,[c] Ye Zhu,[d] Junliang Zhang,[c] Julia A. Mundy,[d] David A. Muller,[d,e] and Frederick T. Wagner[c,*]

[a]*Electrochemical Energy Research Laboratory, General Motors Global R&D, Warren, Michigan 48090, USA*
[b]*Department of Physics, Cornell University, Ithaca, New York 14853, USA*
[c]*Electrochemical Energy Research Laboratory, General Motors Global R&D, Honeoye Falls, New York 14472, USA*
[d]*School of Applied and Engineering Physics, Cornell University, Ithaca, New York 14853, USA*
[e]*Kavli Institute at Cornell for Nanoscale Science, Ithaca, New York 14853, USA*

Advanced electron microscopy techniques, i.e., high angle annular dark field (HAADF) imaging, elemental mapping based on electron energy loss spectroscopy (EELS), and three-dimensional (3D) reconstructions from electron tomography, have been used to characterize the complex spongy core-shell structures observed in a high-performing fuel cell catalyst, a dealloyed $PtCo_3$ catalyst supported on high surface carbon (or D-$PtCo_3$/HSC). HAADF imaging showed that multiple dark-contrast patches were randomly decorated on the D-$PtCo_3$ nanoparticles, a type of image that had previously been reported for other catalysts and had been referred to as a spongy structure. In this work, EELS-based elemental mapping revealed that not all of the dark-contrast patches were simple holes (as had been reported for other catalysts). Rather, in this material, while some of the dark-contrast patches corresponded to voids or divots, others were Co-rich cores. The probability of a dark-contrast patch in an HAADF being a Co-rich core was statistically determined to be 58% ± 15%. 3D tomography further confirmed the existence of voids and divots in the multi-core/shell-structured D-$PtCo_3$ nanoparticles. Possible formation mechanisms of the spongy multi-core/shell structure are discussed.
 [DOI: 10.1149/2.051209jes]

Manuscript submitted May 16, 2012; revised manuscript received June 26, 2012. Published August 14, 2012.

To address environmental and resource-limitation constraints, mainstream automobile companies are striving to put more and more electric vehicles (powered by either lithium-ion batteries[1,2] or proton exchange membrane (PEM) fuel cells[2,3]) on roads in the coming years. To enable PEM fuel cell powered electric vehicles to be cost-competitive with their internal combustion analogs, the development and application of high-performing durable catalysts with a significant cost reduction is paramount.

Platinum (Pt) or Pt-alloy catalysts are still required to adequately catalyze the slow oxygen reduction reaction (ORR) at the cathode of PEM fuel cells. Carbon-supported pure Pt particle catalysts are an industry de facto standard. However, the low activity (0.1 A/mg_{Pt} at 900 mV vs. reversible hydrogen electrode – RHE) of such catalysts means that cathode loadings of ~0.4 mg_{Pt}/cm^2 must be used, leading to a Pt cost per vehicle of several thousands of dollars. To reduce the Pt cost to levels acceptable for mass production of fuel cell vehicles, the activity per unit mass of Pt must be increased at least four-fold.

Pt-alloy catalysts containing base metals such as Co, Ni, Cr, Ti or Cu as the alloying element M and typically with stoichiometry of Pt_3M have historically been demonstrated to outperform pure- Pt catalysts by ~2–3 times in mass activity (on a per-gram basis of Pt).[4–13] The group of Peter Strasser[5,6] showed that higher mass activities could be obtained by starting with nanoparticles containing a higher concentration of the alloying element, e.g., PtM_3, and then removing most of the alloying element via electrochemical voltage cycling prior to measurement of the ORR activity. A similar effect had been reported for thin films, rather than nanoparticles, by the Watanabe group.[14] Koh et al.[5] used this method and synthesized carbon-supported Pt-Cu alloy catalysts which showed a 4–6 fold improvement in mass activity over that of the pure-Pt baseline. They postulated a structure of a pure Pt shell surrounding an alloy core, based on X-ray photoemission spectroscopy showing little of the alloying element in the near-surface region. Dutta et al.[9] confirmed the core-shell structure in dealloyed Pt-Cu alloy catalysts by using high angle annual dark field (HAADF) imaging and electron energy loss spectroscopy (EELS) elemental mapping.

Other structures have also been reported for Pt alloys from which some of the alloying element had been removed by electrochemical cycling or acid leaching. A key factor that controls what structure is formed is the initial base metal atomic fraction before acid leaching or dealloying. Other factors may include temperature, material, overpotential etc. Dahn and coworkers[15] showed that in the case of $Pt_{1-x}M_x$ (M = Fe, Ni, Co, Mn) films, when x is less than 0.6, dissolution of the base metal is primarily from the surface of the alloy, but when x is greater than 0.6, dissolution can extend into the bulk of the film. This suggested that surface dissolution alone (for low base metal fraction) should result in the core-shell structure; surface plus bulk dissolution (for high base metal fraction) will allow massive removal of the base metal and result in porous structure containing voids. Erlebacher et al.[16] have experimentally studied and modeled the structure evolution of surfaces of bulk noble/non-noble metal alloy disks as the non-noble component is electrochemically removed. They showed that a balance between the dissolution rate of the non-noble component and the surface diffusion rate of the noble component can lead to a network of highly crystalline noble-metal ligaments and interconnected pores. Chen et al.[17] showed that both the core-shell structure and a porous "percolated" structure were present in an acid-leached Pt_3Co catalyst (prepared with an initial atomic ratio of Pt:Co close to 1:1 before acid leaching) supported on a high surface-area carbon black. They reported that, while the core-shell structure was present in small and intermediate-sized particles (<10 nm in diameter) in that catalyst, the percolated structure was found to be present mainly in large particles (>10 nm in diameter). A striking morphological feature of the percolated structure was that, in HAADF images, multiple dark-contrast patches were observed within individual large particles.

In this work we studied a Pt-alloy catalyst prepared in our lab with a structural form a bit different from the above-described core-shell and percolated structures. Rather than a core-shell structure with a single Pt-alloy core in each particle, we found a core-shell structure with multiple Pt-alloy cores as well as some voids. We observed dark-contrast patches in the majority (estimated based on HAADF images) of the catalyst particles ranging from small (<5 nm), through intermediate (>5 nm and < 10 nm) to large (>10 nm) diameters. This result, on the particular catalyst that we prepared and studied, differs from Chen et al.'s[17] observation that multiple dark-contrast patches were present only in the large (>10 nm) particles in their commercial catalyst and that all of these dark patches arose from voids. We report our results in detail in this paper.

*Electrochemical Society Active Member.
[z]E-mail: liu_zhongyi@hotmail.com

Experimental

Material.— The chemically dealloyed Pt-Co catalyst supported on high surface carbon (referred to in this paper as D-$PtCo_3$/HSC) was synthesized in our lab. First, a $PtCo_3$/HSC precursor was prepared by impregnating a commercial 28.1 wt% Pt/HSC powder (TKK, Japan) with enough cobalt nitrate solution to give an atomic Pt:Co ratio of 1:3. This precursor was then dried at 70°C in oven for 24 hours. Next, the dried catalyst powder was annealed at 900°C in 10 vol.% H_2/N_2 for 5 hours to reduce the Co and interdiffuse it with the Pt to form a Pt-Co alloy. Finally, the annealed catalyst powder was acid-leached in 1M nitric acid at 80°C for 24 hours to remove the excess Co, forming the final D-$PtCo_3$/HSC catalyst, which had a final stoichiometry of $Pt_{2.7}Co_1$, as measured by inductively coupled plasma atomic emission spectroscopy (ICP-AES). The electrochemical properties of this catalyst, and a comparison to the properties of D-$PtCu_3$, are described in detail elsewhere.[18]

Electron microscopy.— The above-synthesized catalyst powder was dispersed in isopropanol and dropped onto holey-carbon-coated Cu grids suitable for electron microscopy observations. An aberration-corrected Nion UltraSTEM microscope (at Cornell Univ.) was operated at 100 keV in both scanning transmission electron microscopy (STEM) and spectroscopic imaging modes to acquire HAADF images and EELS elemental maps. In the spectroscopic imaging mode, a 33 mrad convergence angle, a typical current of 200 pA, a spatial resolution of ~ 1–1.4 Å, and an energy resolution of 0.35 – 1.0 eV were achieved. Using an additional corrector for improved coupling to the Gatan Enfina spectrometer, electrons scattered up to 77 mrad could be efficiently collected without sacrificing the energy resolution, thereby improving the signal-to-noise of the EELS measurements and enabling faster elemental mapping. The Pt N_3-edge and the Co $L_{2,3}$-edges were recorded simultaneously. A 64×64 pixel map was collected in approximately 10 minutes. To construct the EELS elemental maps, the Co concentration in individual particles was determined using a power-law background[19] subtraction and integration window at the Co $L_{2,3}$ edges. A multivariate curve resolution (MCR)[20] method was used to decouple the Pt signal from the background over a wide energy range (450–650 eV) to allow accurate quantitation despite the breadth and the delayed onset of the Pt N_3 edge. Using this method, a 10-fold increase in Pt signal-to-noise ratio was achieved compared to the results from power-law background subtraction for Pt.[21] Three-dimensional (3D) tomography was performed on an FEI Tecnai F20 microscope (at Cornell Univ.) operated at 200 kV in a STEM mode. By tilting the samples from −67° to +78° with 2° tilt intervals, a series of two-dimensional (2D) images (63.5 nm field of view, 1024 by 1024 pixels) was acquired using an angular dark field (ADF) detector with a collection angle range of 25–150 mrad. The whole series of the 2D ADF/STEM images was manually aligned to a common feature to remove the spatial drift between images at different tilts. The 3D tomographic reconstruction was performed using the simultaneous iterative reconstruction technique (SIRT). This method gives a quantitatively interpretable reconstruction, which is not available through use of filtered results computed with the weighted back projection (WBP) method.[22]

Electrochemical measurements.— The D-$PtCo_3$/HSC catalyst was tested on rotating disk electrodes (RDE) in a three-electrode cell at room temperature. An Ag/AgCl/KCl (3 M Cl^-) leak-free electrode was used as a reference; a platinum flag was employed as the counter electrode; and 0.1 M perchloric acid ($HClO_4$) was used as the electrolyte. The potentials in the RDE tests are reported relative to RHE. A catalyst ink consisting of 15 mg catalyst powder, 12 mL H_2O, 3 mL iso-propanol, and 0.06 mL of a 5 wt% ionomer solution (water/n-propanol weight ratio = 1:1, DuPont, USA) was sonicated for 10 minutes. Then, 10 μL of the catalyst ink was pipetted onto a flat glassy carbon electrode (5-mm diameter, Pine Instrument, USA) to achieve a Pt loading of 15 μgPt/cm^2. This electrode was then dried in a weak N_2 flow for 3 hours. The resulting catalyst layer on the glassy carbon electrode was first cleaned by cycling the voltage from 0.05 to 1.2 V at the rate of 1 V/s for 200 cycles. After this cleaning step, it was assumed that no further structural change would occur during the RDE testing possibly due to the aggressive acid leaching used in the initial de-alloying step. Then the ORR measurement was carried out via an anodic scan from 0.05 to 1.1 V at a rate of 5 mV/s, while pure O_2 was bubbled through the electrolyte. The catalytic activity of catalysts is expressed in terms of Pt mass activity (MA) in A/mg_{Pt} or specific activity (SA) in μA/cm^2_{Pt} at 0.9 V. The reported RDE activity is the result of averaging data from 3 electrodes made from each of two inks.

Table I. Comparison of electrochemical properties (HAD, MA and SA) between of the D-$PtCo_3$ catalyst and pure-Pt catalyst measured by RDE.

	D-PtCo3/HSC	Pt/Vulcan (baseline)
HAD (m^2/g_{pt})	62.5	56.0
Mass activity (A/mg_{Pt})	0.40	0.13
Specific activity (μA/cm^2_{Pt})	634.5	233.0

Results and Discussion

The mass activity of the D-$PtCo_3$/HSC catalyst was about 0.4 A/mg_{Pt}, which is 3-4 times higher than that of the pure-Pt catalyst baseline. Detailed electrochemical properties (i.e, MA and SA); and HAD - hydrogen adsorption desorption area (electrochemically accessible surface area)) of this catalyst and those of the pure-Pt catalyst baseline for comparison are given in Table I.

Fig. 1 shows the particle size and size distribution of the D-$PtCo_3$/HSC measured from HAADF images of the fresh, dealloyed catalyst powder. The particle size is about 3.9 nm (number-averaged) or 5.9 nm (volume-surface area – averaged).

Figs. 2a-2c show typical HAADF images of the fresh, dealloyed D-$PtCo_3$ nanoparticles. In Figs. 2a-2c, two clear observations are i) dark-contrast patches are present in the nanoparticles; and ii) their presence is particle size – independent, that is, they are present in small (< 5 nm), intermediate (> 5 nm and <10 nm) and large (> 10 nm) nanoparticles. Fig. 2c highlights one intermediate-sized particle that has dark-contrast patches. Note that no dark-contrast patches were observed in any of the HAADF images taken from $PtCo_3$ precursor nanoparticles before acid leaching. As an example Fig. 2d gives a pre-dealloying HAADF image which shows a uniform contrast in all of the $PtCo_3$ precursor nanoparticles.

Fig. 3 shows a variety of the types of HAADF images and EELS maps obtained from the D-$PtCo_3$ nanopaticles (a larger set than shown

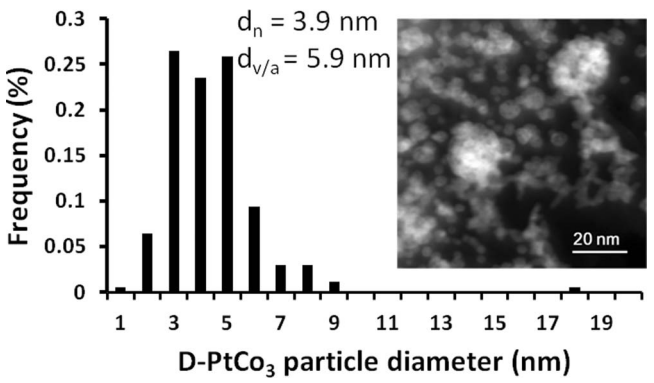

Figure 1. Particle size distribution of the fresh, dealloyed D-$PtCo_3$ nanoparticles measured from HAADF images (a typical HAADF image is shown in the inset. Also shown are particle sizes that are number-averaged (3.9 nm) or a volume-surface-area-averaged (5.9 nm).

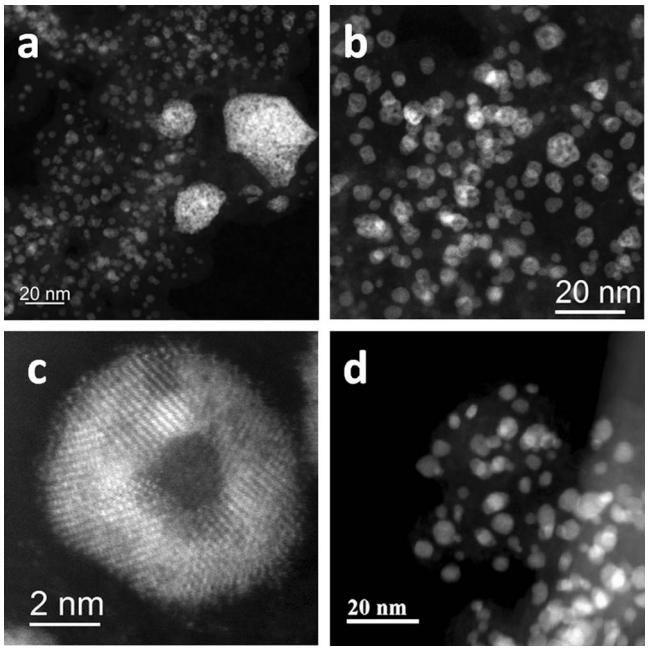

Figure 2. a-c: HAADF images showing dark-contrast patches present in small (<5 nm), intermediate (> 5 nm and <10 nm), and large (>10 nm) particles of the fresh, dealloyed D-$PtCo_3$ catalyst powder. d: HAADF image showing a uniform contrast (or no dark-contrast patches for comparison with a-c) present in the precursor $PtCo_3$ nanoparticles before acid leaching.

here was imaged). The colors in the EELS maps correspond to specific elements, i.e., red for Pt, green for Co, with mixtures of Pt and Co showing up as yellow. Three recurrent situations in the images of Fig. 3 are exemplified in Figs. 4-6: *i*) Fig. 4: dark-contrast patches are Co-rich pockets; *ii*) Fig. 5: dark-contrast patches are voids/divots (absence of Co and Pt); and *iii*) Fig. 6: dark-contrast patches are an overlap of Co-rich region and a void/divot. A detailed discussion of these observations follows.

Fig. 4 shows an intermediate-sized nanoparticle (> 5 nm and <10 nm). Some of the dark-contrast patches are highlighted with white

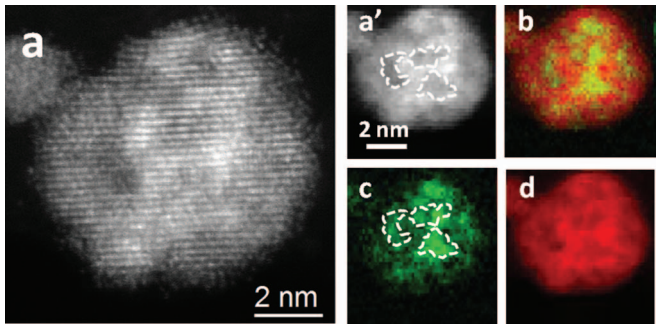

Figure 4. Simultaneously recorded HAADF image (a′) and EELS maps (b-composite, c-Co, d-Pt) from a fresh, dealloyed D-$PtCo_3$ nanoparticle. Another HAADF image (a) recorded with the same probe settings, but higher pixel density than the HAADF image (a′) and the EELS maps. Lattice fringes are clearly visible in the HAADF image (a). The patches with a dark contrast are highlighted by dotted lines in the HAADF image (a′) and corresponding locations are also highlighted the same way in the Co map (c). It is clearly seen that these dark contrast patches are Co-rich pockets.

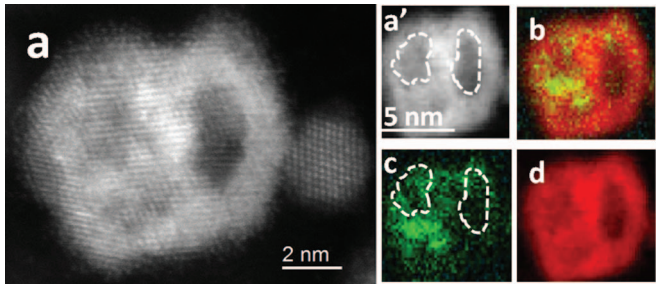

Figure 5. Simultaneously recorded HAADF image (a′) and EELS maps (b-composite, c-Co, d-Pt) from a fresh, dealloyed D-$PtCo_3$ nanoparticle. Another HAADF image (a) recorded with the same probe settings, but higher pixel density than the HAADF image (a′) and the EELS maps. Lattice fringes are clearly visible in the HAADF image (a). The dark-contrast patches (highlighted by dotted lines in a′ and c) show the absence of Co and Pt, suggesting that this patch is a void/divot.

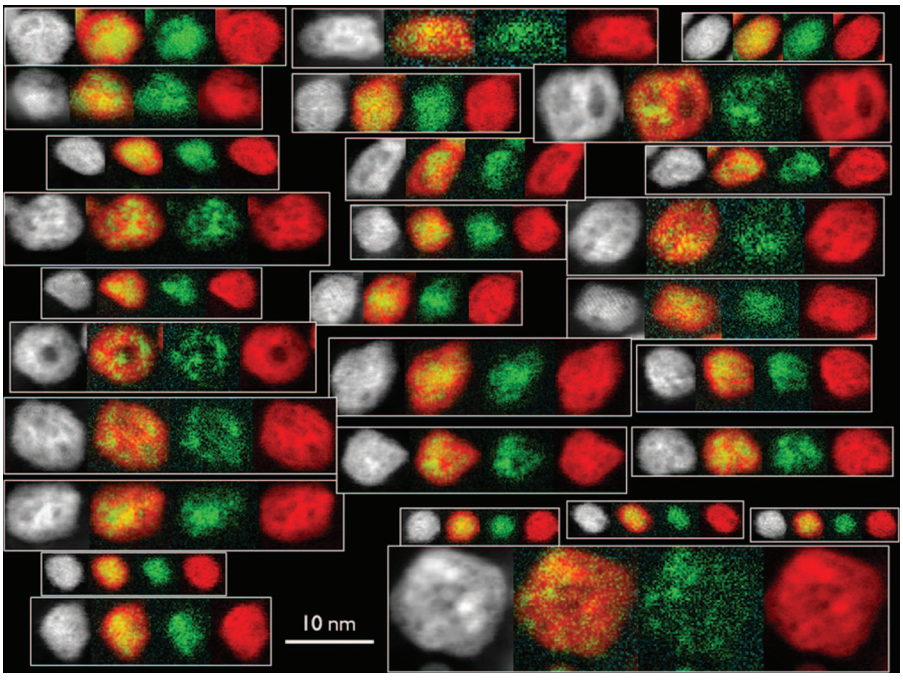

Figure 3. HAADF images (gray) and EELS maps (red-Pt, green-Co, yellow-composite or mixture of Pt and Co) obtained from the fresh, dealloyed D-$PtCo_3$ nanoparticles.

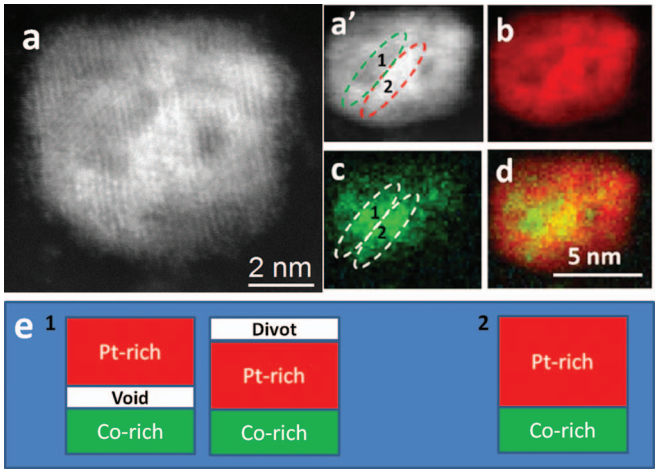

Figure 6. Simultaneously recorded HAADF image (a′) and EELS maps (b-Pt, c-Co, d-composite) of a fresh, dealloyed D-$PtCo_3$ nanoparticle. Another HAADF image (a) recorded with the same probe settings, but higher pixel density than the HAADF image (a′) and the EELS maps. Lattice fringes are clearly visible in the HAADF image (a). Two adjacent patches (indicated by 1 and 2) are highlighted in the HAADF image (a′) and in the Co map (c). While the contrast of these two patches is different in the HAADF image (a′), their intensities are qualitatively the same in the Co map (c). The difference in HAADF, but not Co intensity can be explained by the illustrations in (f), with two scenarios for region 1 and one for region 2. In f, the Pt-rich region is in red, the Co-rich region is in green, and the void or divot is in white.

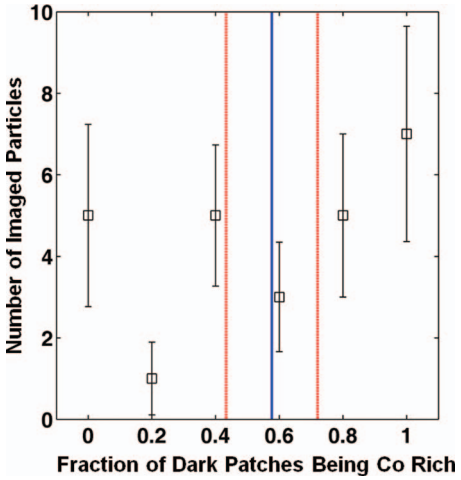

Figure 7. A Plot showing a 58% ± 15% probability of the dark-contrast patches being Co-rich pockets in the fresh, dealloyed D-$PtCo_3$ nanoparticles. The blue and red lines show mean (58%) and 95% confidence interval (15%), respectively.

dotted lines in the HAADF image (Fig. 4(a′)); and the corresponding locations of these patches in the Co map (Fig. 4c) are also outlined. It is clear that the dark-contrast patches are regions with a significant presence of Co. The dark contrast in the HAADF image is due to the scattering of Co being weaker than that of Pt (proportional to $Z^{\sim 1.7}$) according to the Rutherford formula for scattering from an unscreened nucleus.[23] It is also clear from Fig. 4 that this nanoparticle has a non-uniform Pt-Co alloy core with several local concentrations of Co (suggested by the green [Co map, Fig. 4c] and yellow [Co and Pt composite map, Fig. 4b] regions.)

Fig. 5 shows a large nanoparticle (>10 nm in diameter). In the HAADF images (Figs. 5a and 5(a′)), this nanoparticle also has a similar morphology of the dark-contrast patches to that shown in Fig. 4. Two dark-contrast patches are highlighted with white dotted lines in the HAADF image (Fig. 5(a′)) and the Co map (Fig. 5c). When qualitatively comparing the Co intensity of these two patches to that of the adjacent region, a difference can immediately be seen, i.e., Co and Pt are absent in these dark-contrast patches. This suggests that each of these dark-contrast patches may be a void (in the bulk) or a divot (hole at the surface). Differentiation of a void from a divot can be made via 3D tomography, which will be discussed later in this paper.

Fig. 6 shows subtler situations than those showed in Figs. 4 and 5. The HAADF images (Figs. 6a and 6(a′)) shows a particle (∼10 nm in diameter) with one dark-contrast and one bright-contrast patch (highlighted in Fig. 6(a′)) by green and red dashed lines, respectively). These patches are adjacent to each other. While the contrast of these two patches is different in the HAADF image (a′), their intensities are qualitatively the same in the Co map (c). A possible reason is illustrated in Fig. 6e. In this figure, the Pt-rich region is in red, the Co-rich region is in green, and the void or divot is in white. Two scenarios A and B are shown in Fig. 6e with the direction of the electron beam coming down from the top of the page. Scenario A consists of 1) a Pt-rich region, a void, and a Co-rich region which overlap one another, or of 2) a divot, a Pt-rich region, and a Co-rich region [equivalent to 2), a Pt-rich region, a Co-rich region, and a divot]. Scenario B consists of a Pt-rich region and Co-rich region which overlap each other (no void/divot is present in Scenario B). If the thickness effect of the void is negligible (this is a reasonable assumption since the thickness of the void is in the regime of less than a couple of nanometers), Scenario A will generate less intensity in HAADF than Scenario B; but, qualitatively speaking, Scenarios A and B will produce the same intensity in the Co map.

We further determined the probability of the dark-contrast patches being either a Co-rich core or a void/divot from EELS maps of over 30 D-$PtCo_3$ nanoparticles with varying particle sizes. Fig. 7 shows the statistical results. For 26 particles that were analyzed, the number of particles (N) and the probability (%) to see dark-contrast patches being Co-rich were as follows: 7 (100%), 5 (80%), 3 (60%), 5 (40%), 1 (20%), and 5 (0%). Based on this analysis, the probability to see dark-contrast patches that are Co-rich in a particle is 58% (mean, blue line in Fig. 7) ± 15% (95% confidence interval, red lines in Fig. 7)), vs. 42% for void/divots. Note that the correlation (if any) between these statistics and the particle size of these D-$PtCo_3$ nanoparticles has not been explored in this work.

It is worthwhile noting that some D-$PtCo_3$ nanoparticles having a core-shell structure with a single Pt-Co core were also observed in this work (e.g., small nanoparticles shown on the bottom right of Fig. 3 and in Fig. 8). These core-shell nanoparticles were often small in diameter

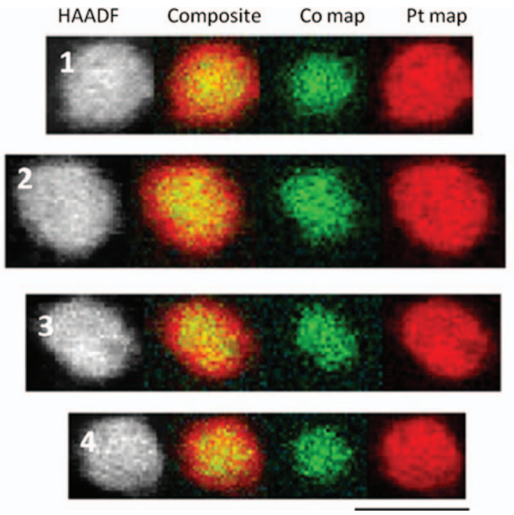

Figure 8. Four small (<5 nm) D-$PtCo_3$ nanoparticles shown as HAADF, composite, Co map, and Pt map (in a row for each particle). A core-shell structure with a single core is seen from these nanoparticles. The scale bar is 5 nm.

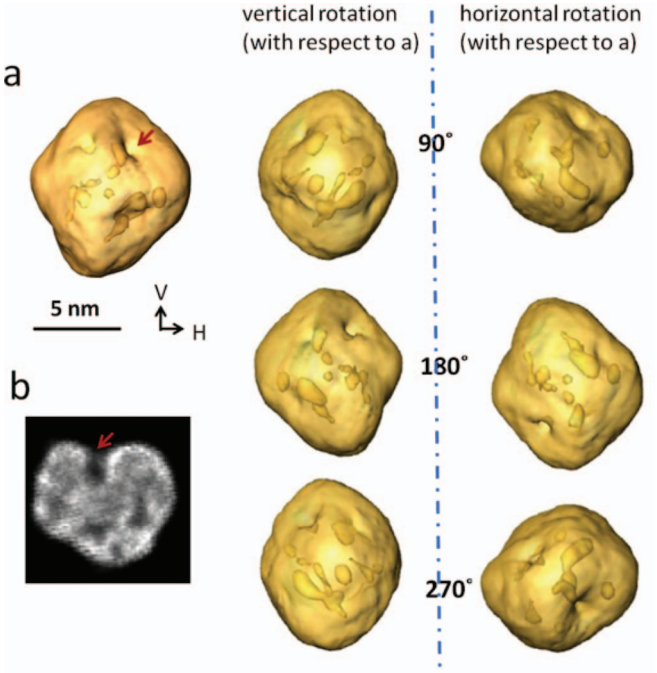

Figure 9. a: A 3D tomographic reconstraction of a fresh, dealloyed D-$PtCo_3$ nanoparticle (~ 10 nm in diameter) and this reconstruction viewed at 90°, 180°, and 270° rotation in vertical and horizontal axes. The irregular discrete regions within the 3D reconstruction corresponding to the dark-contrast patches shown in the HAADF images obtained earlier from this material. b: An isosurface [an image obtained by cross-sectioning the 3D reconstruction at a certain angle that a divot (indicated by red arrows in both a and b) is well visualized]. This isosurface also shows that the shell has a brighter contrast (which is contributed by Pt) than the core. This clearly suggests that the D-$PtCo_3$ nanoparticle has a Pt-shell / Pt-Co-core structure.

(5 nm or less) and represented a small fraction of all of the D-$PtCo_3$ nanoparticles observed. The shell thickness was 2-3 monolayers of Pt, which is similar to the Pt shell thickness of core-shell structured catalyst nanoparticles seen after acid leaching of a commercial Pt_3Co catalyst.[17] The formation of this core-shell structure may be due to local composition variations of the D-$PtCo_3$ precursors before acid leaching (please recall that low base metal atomic fraction leads to dissolution only from the surface and a resulting simple Pt-shell/alloy-core structure[15]).

To determine whether the dark-contrast patches are voids (in the bulk) or divots (at the surface of a nanoparticle), 3D tomography was performed. Fig. 9 shows a 3D tomographic reconstruction and the reconstruction rotated to 90°, 180°, and 270° in both vertical and horizontal axises. Also shown in Fig. 9 is an isosurface of the 3D reconstruction (i.e., a 2D image obtained by cross-sectioning/surface-cutting the 3D reconstruction at an angle at which a divot is best visualized). The 3D reconstruction (Fig. 9a) shows multiple irregular discrete regions within the nanoparticle. These regions correspond to dark-contrast patches in HAADF images. It is clear from the EELS maps that the dark-contrast patches are either Co-rich cores or Co-and-Pt-absent voids or divots. There is one region in particular (indicated by a red arrow) that has a channel connecting to the exterior surface of the nanoparticle. This region is actually a divot which is indicated by a red arrow in the isosurface Fig. 9b. The isosurface (Fig. 9b) also shows that the shell of the nanoparticle has a brighter contrast (which is contributed by Pt) than the core. This clearly suggests that the D-$PtCo_3$ nanoparticle has a Pt-shell / Pt-Co-core structure. The shell thickness is about 3 monolayers of Pt, which is consistent with the Pt shell thickness of the few single-core/shell structured nanoparticles (shown in Fig. 8). Based on the 3D tomography and earlier HAADF and EELS results, one can conclude that the D-$PtCo_3$ nanoparticles have a spongy multi-core/shell structure after acid leaching.

How does the spongy multi-core/shell structure form? To answer this question, we first discuss the formation mechanism of the spongy structure in bulk materials. The formation mechanism in bulk Ag-Au alloys was elegantly established by Erlebacher et al.[16] The key points of this mechanism are *i*) atom-by-atom surface dissolution of Ag and Au cluster formation via surface aggregation driven by capillarity-driven surface diffusion of Au lead to the formation of a pit at the surface; *ii*) as the pit proceeds laterally into sufficient surface area and vertically into sufficient depth, new Au cluster nucleates and the parent pit splits into multiple child pits; *iii*) the child pits continue to multiply and penetrate into the bulk until a full, three-dimensional porous structure forms. In contrast to the Ag-Au etc. bulk materials, the D-Pt_3Co alloy studied here were nanometer-structured particles (ranging from a few to tens of namometers in diameter). The complex spongy multi-core/shell structure could stem from the interplay of acid leaching and the effects of the particle size and size-related features such as local composition variation, surface curvature, and defects). However, just how they impact the formation of this complex structure of the D-$PtCo_3$ nanoparticles requires further investigation.

It should be noted that in recent work by Oezaslan et al.[24] the authors indicated that the morphologies of their dealloyed Pt-Co and Pt-Cu nanoparticles have a strong dependence on particle size. They concluded that there are two characteristic diameters, $d_{multi\text{-}cores}$ (10–15 nm) and d_{pores} (30 nm) which correspond to three length regimes [i.e., i) below 10–15 nm, ii) between 10–15 nm and 30 nm, and iii) above 30 nm], where single core-shell, multi-core/shell, and porous multi-core/shell nanoparticles form, respectively. In the present work, a relatively large number of particles were examined in detail, but we did not explicitly address whether such a correlation between particle size and morphology exists.

Conclusions

HAADF images, EELS elemental maps, and 3D tomography have revealed that a complex spongy multi-core/shell structure is present in the 30% D-$PtCo_3$/HSC catalyst nanoparticles synthesized in our lab. EELS elemental maps have clearly shown that HAADF images that appear "spongy" are not always indicative of pores within the particles. While some dark-contrast patches are voids/divots (i.e., really spongy because of the absence of both Co and Pt), others are solid but Co-rich cores. In the catalyst studied here, the averaged probability to observe patches that were Co-rich was determined to be 58% ± 15%. This work differs from the earlier observations (e.g., Chen et al.[17] and Oezslan et al.[24]) in the Co content of the Pt-Co precursors, in the predominance of particles with multiple dark-contrast patches, and in the positive identification of both voids and Co-rich cores in the multiple dark-contrast-patched particles. Future work will discuss possible correlations between the detailed structures reported here and the activity and durability of these 30% D-$PtCo_3$ catalysts. Pt-alloy catalysts in general will likely have, in use, various kinds of core/shell structures. It is of critical importance to understand where the alloying-element atoms should best be located with respect to the Pt surface to confer durably high activity.

Acknowledgments

This work was supported in part by the United States Department of Energy, Office of Energy Efficiency and Renewable Energy, under Contract DE-EE0000458. Financial support of the work at Cornell University from NSF-CNS and Semiconductor Research Corporation is gratefully acknowledged.

References

1. R. F. Service, *Science*, **324**, 1257 (2009).
2. F. T. Wagner, B. Lakshmanan, and M. F. Mathias, *J. Phys. Chem. Lett.*, **1**, 2204 (2010).
3. M. F. Mathias, R. Makharia, H. A. Gasteiger, J. J. Conley, T. J. Fuller, C. J. Gittleman, S. S. Kocha, D. P. Miller, C. K. Mittlesteadt, and T. Xie, et al., *Electrochem. Soc. Interface*, **14**, 24 (2005).
4. V. Stamenkovic, B. S. Mun, M. Arenz, K. J. J. Mayrhofer, C. A. Lucas, G. Wang, P. N. Ross, and N. M. Markovic, *Nature Mater.*, **6**, 241 (2007).

5. S. Koh and P. Strasser, *J. Am. Chem. Soc.*, **129**, 12624 (2007).
6. P. Mani, R. Srivastava, and P. Strasser, *J. Phys. Chem. C*, **112**, 2770 (2008).
7. J. X. Wang, H. Inada, L. Wu, Y. Zhu, Y. Choi, P. Liu, W.-P. Zhou, and R. R. Adzic, *J. Am. Chem. Soc.*, **131**, 17298 (2009).
8. M. K. Debe, A. K. Schmoeckel, G. D. Vernstrom, and R. Atanasoski, *J. Power Sources*, **161**, 1002 (2006).
9. I. Dutta, M. K. Carpenter, M. P. Balogh, J. M. Ziegelbauer, T. E. Moylan, M. H. Atman, and N. P. Irish, *J. Phys. Chem. C.*, **114**, 16309 (2010).
10. J. Wu, J. L. Zhang, Z. Peng, S. Yang, F. T. Wagner, and H. Yang, *J. Am. Chem. Soc.*, **132**, 4984 (2010).
11. T. Ghosh, M. B. Vukmirovic, F. J. DiSalvo, and R. R. Adzic, *J. Am. Chem. Soc.*, **132**, 906 (2010).
12. C. Wang, M. Chi, G. Wang, D. Vliet, D. Li, K. L. More, H. Wang, J. A. Schlueter, N. M. Markovic, and V. R. Stamenkovic, *Adv. Funct. Mater.*, **21**, 147 (2011).
13. P. Strasser, S. Koh, Toyli Anniyev, J. Greeley, K. More, C. Yu, Z. Liu, S. Kaya, D. Nordlund, H. Ogasawara, M. F. Toney, and A. Nilsson, *Nature Chem.*, **2**, 454 (2010).
14. T. Toda, H. Igarashi, H. Uchida, and M. Watanabe, *J. Electrochem. Soc.*, **146**, 3750 (1999).
15. A. Bonakdarpour, R. Lobel, R. T. Atanasoski, G. D. Vernstrom, A. K. Schmoeckel, M. K. Debe, and J. R. Dahn, *J. Electrochem. Soc.*, **153**, A1835 (2006).
16. J. Erlebacher, M. J. Aziz, A. Karma, N. Dimitrov, and K. Sieraszki, *Nature*, **410**, 450 (2001).
17. S. Chen, H. A. Gasteiger, K. Hayakawa, T. Tada, and Y. Shao-Horn, *J. Electrochem. Soc.*, **157**, A82 (2010).
18. Z. Yu, J. L. Zhang, Z. Y. Liu, J. M. Ziegelbauer, H. L. Xin, J. A. Mundy, D. A. Muller, and F. T. Wagner, *J. Phys. Chem. C*, in press.
19. R. F. Egerton, *Phil. Mag.*, **31**, 199 (1975).
20. R. Tauler, A. Izquierdoridorsa, and E. Casassas, *Chemometrics Intell. Lab. Syst.*, **18**, 293 (1993).
21. H. L. Xin, J. A. Mundy, Z. Y. Liu, R. Cabezas, R. Hovden, L. F. Kourkoutis, J. L. Zhang, N. P. Subramanian, R. Makharia, F. T. Wagner, and D. A. Muller, *Nano Lett.*, **12**, 490 (2012).
22. P. A. Midgley and M. Weyland, *Ultramicroscopy*, **96**, 413 (2003).
23. M. M. J. Treacy and J. M. Gibson, *Ultramicroscopy*, **52**, 31 (1993).
24. M. Oezaslan, M. Heggen, and P. Strasser, *J. Am. Chem. Soc.*, **134**, 514 (2012).